INVESTIGATIONS ON HIGH REYNOLDS NUMBER LAMINAR FLOW AIRFOILS

G. Redeker K.H. Horstmann
H. Köster A. Quast
Deutsche Forschungs- und Versuchsanstalt für Luft- und Raumfahrt e.V. (DFVLR), Institut für Entwurfsaerodynamik
D-3300 Braunschweig, Fed. Rep. Germany

Abstract

For further operating-cost reduction on transport aircraft drag reduction by extended laminar flow on wings and empennages is mandatory. With carefully designed airfoils laminar flow can be achieved even at high Mach- and Reynolds numbers and moderate sweep angles. With laminar airfoils operating-cost decrease in the order of 30 %. Two- and three-dimensional stability theory seems to be a good tool for determining laminar-turbulent boundary layer transition caused by Tollmien-Schlichting and crossflow instabilities but it has to be checked by extensive flight tests because windtunnel tests are not well suited as a consequence of the micro-turbulence of the flow and windtunnel noise.

Notation

c	m	airfoil chord length
c_d	-	drag coefficient airfoil
c_ℓ	-	lift coefficient airfoil
c_L	-	lift coefficient wing
c_p	-	pressure coefficient
L/D	-	lift to drag ratio
M	-	Mach number
M_F	-	flight Mach number
N_{CFI}	-	amplification exponent for crossflow instability
N_{TSI}	-	amplification exponent for Tollmien-Schlichting instability
Re	-	Reynolds number
U_e	m/s	stream velocity at the boundary layer edge
V_∞	m/s	undisturbed flow velocity
x	m	streamwise coordinate
x/c	-	fraction of chord
y	m	coordinate perpendicular to streamlines
z	m	coordinate perpendicular to wing surface
α	degree	angle of attack
Λ	-	aspect ratio of wing
φ	degree	sweep angle

1. Introduction

Increasing fuel prices in the past and the long-term forecast of further rising energy cost and after all the strong competition among the airlines are the incentives for the development of new commercial transport aircraft with remarkable reduction in fuel consumption and increased economic operation. By new technologies in aerodynamics drag reduction is possible by increasing the part of the laminar boundary layer on a wing surface thus reducing skin friction drag considerably. Low drag airfoils or laminar airfoils have been used extensively since years in gliders and very low drag coefficients have been achieved compared to those of conventional airfoils used for transport aircraft, as it is demonstrated in Fig. 1. Here, two drag polars of different airfoils are compared. The first one is the laminar airfoil DFVLR-HQ35 designed for a glider and the second one is the transonic airfoil DFVLR-R4, well-suited for a transport aircraft. The extremely low drag coefficient c_d of the glider airfoil is mainly due to the reduction of skin friction by long extension of laminar boundary layers on upper and lower airfoil surface. This long extension of the laminar boundary layer is promoted by specially tuned pressure distributions and by the low Reynolds numbers ($Re \approx 2 \cdot 10^6$) of gliders. Airfoils for transonic aircraft operate at substantially higher Reynolds- and Mach numbers and exhibit pressure distributions which have been designed according to transonic flow. These pressure distributions lead at

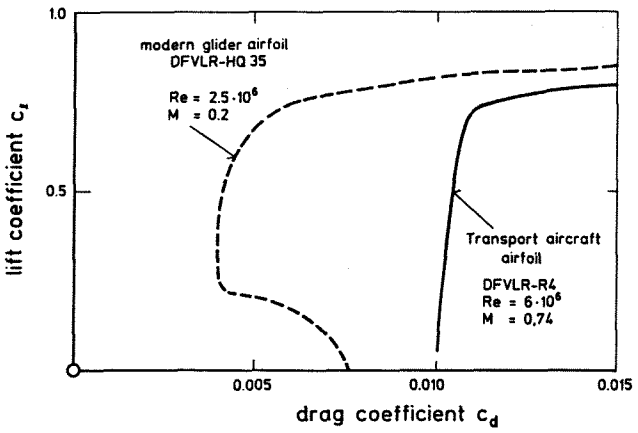

Fig. 1 Comparison of drag polars between airfoils of present transport aircraft and modern gliders

Reynolds numbers of $Re \approx 20 \cdot 10^6$ in combination with swept wings to fully turbulent boundary layers which results in a higher drag coefficient. From Fig. 1 it can be seen that the drag coefficient c_d of the glider airfoil is only 40 % of the transonic airfoil drag in a reasonable region of lift coefficients. The present paper deals with the possibility to extend the technology of natural laminar flow to higher Reynolds- and Mach numbers and to the case of swept wings. In the following a short description of the transition mechanisms from laminar to turbulent boundary layers on swept wings will be given and the methods used for designing such airfoils will be outlined including guidelines for the design. A design example will be discussed together with the resulting improvement for a transport aircraft. Finally some of the problems arising with this new technology will be addressed.

2. Transition from laminar to turbulent boundary layers on swept wings

Studies of economic operations of transport aircraft show that a high value of cruise speed times lift/drag ratio is necessary. As the lift/drag ratio of transport aircraft is nearly independent from the cruise speed, as long as no undesirable transonic effects occur, the highest velocity possible is the basis for a good economic operation. This leads to swept wing planforms for transonic transport aircraft, which also have to be realized when applying laminar airfoils.

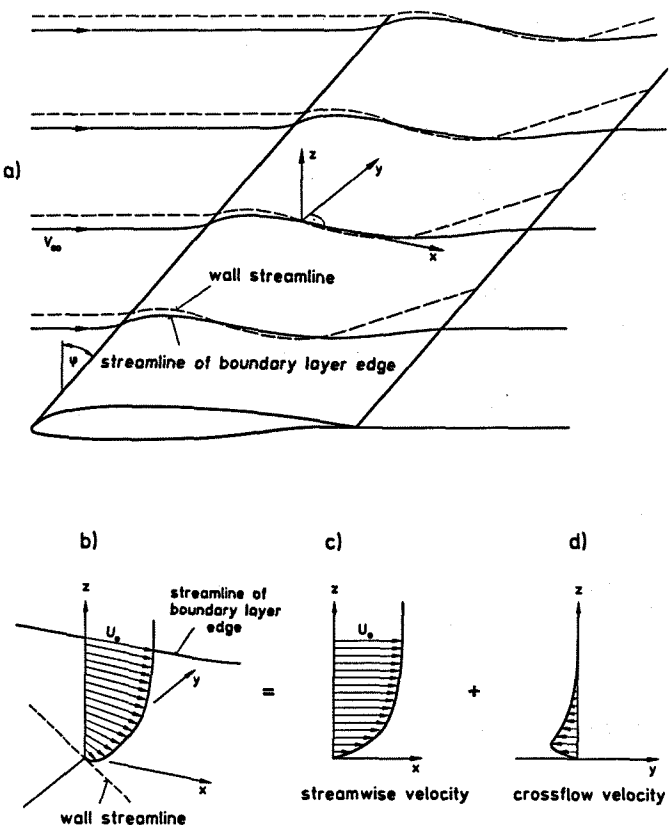

Fig. 2 Flow pattern and boundary layer velocity distribution on an infinite swept wing

Due to the sweep angle the boundary layer on swept wings becomes highly three-dimensional and additional effects can cause boundary layer transition. Fig. 2 gives an overview of the flowfield in the boundary layer of a swept wing. In the simple case of an infinite swept wing the incoming flow can be split up in spanwise direction and normal to it. The flow component in spanwise direction remains constant over the wing forming an attachment line at the leading edge with a finite velocity. The streamlines of the potential flow over the wing are highly curved in the planform plane at the leading edge region as a result of pressure gradients acting transverse to the local flow direction. Due to the presence of a boundary layer with zero velocity at the wing surface the curvature of the wall streamlines is different from that of the potential flow, as it is indicated in Fig. 2 by the full and the dotted lines. This behaviour leads to skewed velocity profiles in the boundary layer, where the flow direction is changing with the distance to the wall from the direction of the wall streamline to the direction of the potential flow streamline. Splitting up these velocity profiles in the direction of the outer flow and perpendicular to it one ends up into two velocity profiles also given in Fig. 2. The first profile in direction of the outer flow is very similar to that of a two-dimensional boundary layer, whereas the second one shows a different shape. This so-called crossflow distribution is characterized by a maximum near the surface decreasing to zero velocity at the surface and at the outer edge of the boundary layer including always a point of inflexion.

These complicated flow patterns in the boundary layer especially in the leading edge region influence the transition of the laminar boundary layer on swept wings considerably. Essentially the following three transition mechanisms or combinations of them can occur:

- transition due to Tollmien-Schlichting instability (TSI) as known from the two-dimensional case
- transition due to crossflow instability (CFI)
- attachment line transition (ALT).

The boundary layer profile in the direction of the outer flow is very similar to that of a two-dimensional boundary layer and therefore Tollmien-Schlichting waves [1] can occur which leads through a complicated process to transition into a turbulent boundary layer. The main parameter which influence the occurence of unstable oscil-

lations are pressure distribution and Reynolds number.

Early experiments on swept wings [2,3,4] showed a premature transition near the leading edge on smooth swept wings and detailed investigations indicated that the instability of the crossflow velocity profiles caused boundary layer transition. As these velocity profiles always have an inflexion point one can show from stability analysis considerations that the instability of such type of profiles is larger than those of the usual ones [5]. The main parameters which are influencing the crossflow instability are sweep angle, Reynolds number and pressure distribution.

Within the boundary layer of the attachment line flow spanwise turbulent contamination can occur [6,7] induced by an inherent instability of the boundary layer or by leading edge roughness. This behaviour results in a fully turbulent boundary layer over the whole wing surface. Attachmentline transition is dependent on sweep angle, Reynolds number, leading edge radius and acceleration of the flow in the attachment line region. Criteria for avoiding this kind of transition have been reported in [6,7]. Thus, crossflow instability and attachment line transition are highly important and special attention has to be paid to these phenomena when designing laminar airfoils for swept wings.

3. Design of natural laminar flow airfoils for swept wings

3.1 Methods for design

The most critical point when designing natural laminar flow airfoils for swept wings at high Reynolds numbers is the prediction of transition location. For low Reynolds numbers ($Re \approx 3 \cdot 10^6$) and sweep angles of $\varphi = 0^\circ$ very efficient empirical relations have been derived [8,9] from a large data base of experiments. For higher Reynolds numbers only few experiments exist to prove these criteria. For attachment line transition also empirical relations after [6,7] seem to work satisfactory. Empirical relations for determining transition due to crossflow instability have been established in [10,11]. As the experimental data base to prove these criteria is very small these relations seem not to be adequate to serve as a realistic tool in the design of high Reynolds number airfoils for swept wings. A more sophisticated approach to determine transition location is the use of the stability theory of laminar boundary layers [1,12,13]. We refer here to the work presented in [5,14], where a stability analysis on the basis of the temporal stability theory for boundary layers on swept wings has been described. The basic idea is the investigation of the amplification of disturbances in the form of waves within the boundary layer. The governing three-dimensional disturbance equations [15] derived from the Navier-Stokes equations can be reduced to a single quasi-two-dimensional disturbance equation in the direction of the disturbance wave front, which in the three-dimensional case is normally not in the direction of the local flow. This equation known as Orr-Sommerfeld-equation [1] was derived in [15] for the direction normal to the wave front. It can be applied according to [15] to the three-dimensional stability problem by solving a series of two-dimensional problems with various wave propagation angles. Solutions of this equation are obtained by solving an eigenvalue problem and are described in [5] by employing a computer code SALLY for incompressible, three-dimensional parallel flow.

This code allows the calculation of amplification rates of disturbances of various wave lengths, frequencies and different disturbance propagation directions. From these amplification rates the amplification ratio can be determined. If it is assumed, that a disturbance has an amplitude A_o when it starts amplifying first, then the amplification ratio A/A_o at any point can be calculated by integrating the amplification rate up to that point. This amplification ratio can be expressed by an exponential function e^N where N is the amplification exponent or N-factor. It describes the growth of the oscillations and will be related to the transition condition. This procedure must be carried out for those oscillation frequencies, wave lengths and wave propagation directions, where the amplification exponent N becomes a maximum of all oscillations.

When analysing the boundary layer of swept wing pressure distributions it turns out that in principle two wave front propagation directions are important. The first one is related to wing regions with weak pressure gradients, where the disturbances are propagating nearly in the direction of the outer flow, corresponding to the two-dimensional type of Tollmien-Schlichting instability. The second one is related to the wing region with strong pressure gradients near the leading edge, where the disturbances of maximum amplification are propagating in the crossflow direction, corresponding to the crossflow instability.

Fig. 3 gives an example of a stability analysis of experiments taken from [4] on a swept wing. The left part of the figure shows the pressure distributions of a 20° swept wing at $M = 0.27$ and $Re = 15 \cdot 10^6$ at different angles of attack, which have been analysed with the SALLY-code [5,14] in the Tollmien-Schlichting mode as well as in the crossflow mode. The middle part of the figure presents the amplification exponents N_{TSI} of the Tollmien-Schlichting instability as an envelope of various frequencies investigated along the wing chord. TS-instability first starts after a certain distance from the leading edge (app. 8 % of local chord) and the N_{TSI}-curve is increasing

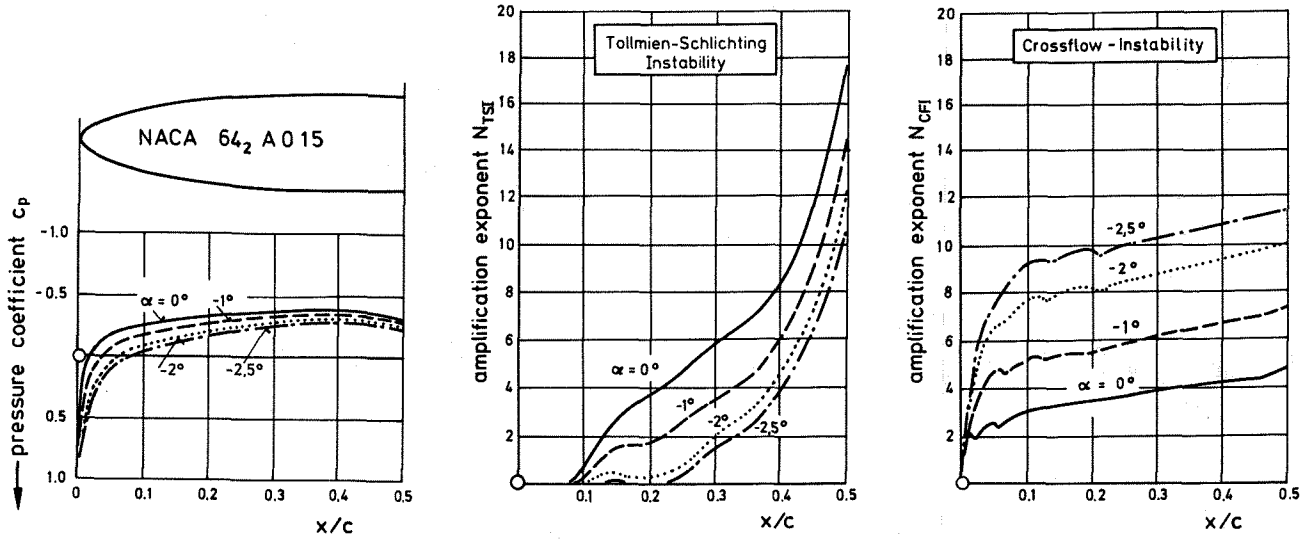

Fig. 3 Tollmien-Schlichting and crossflow instability for NACA 64_2A015 airfoil upper side for different angles of attack, M = 0.27, Re = $15 \cdot 10^6$, $\varphi = 20°$

steadily. In the right part of the figure amplification exponents N_{CFI} due to crossflow instability have been plotted at zero frequency describing stationary waves which have also been detected in experiments. Here one can see that the amplification of the disturbances starts immediately at the leading edge with a steep increase in the region of large pressure gradients. In the following part of the pressure distribution with weak gradients only a small increase in values of N_{CFI} can be seen. In the calculation with the SALLY-code no interaction between crossflow- and Tollmien-Schlichting instability can be taken into account.

To proceed to the transition location from this stability analysis results the usual way is to determine the calculated N-factors at the experimental transition locations, thus establishing a limiting N-value. The various N-factors for transition from different publications and experiments do not show a clear picture [16,17,18]. It seems to be reasonable that for TS-instability transition is likely to occur at $N_{TSI} = 11$ in low turbulence windtunnels and $N_{TSI} \approx 18$ in flight experiments.

The crossflow N-values in windtunnels reach values of $N_{CFI} \approx 9$ to 11 [5,16], whereas no real flight data are available. For our following design example $N_{TSI} = 18$ and $N_{CFI} = 12$ have been assumed. The airfoil design has been carried out by a combined procedure using the subsonic design method of Eppler/Somers [18] together with a modified version of the BGKJ-code [19]. The transition location at the critical points was checked with the SALLY-code as it has been described before.

3.2 Design features

The drag of a laminar flow airfoil is mainly depending on the extent of the laminar boundary layer on both airfoil surfaces. Thus, the aim of the design process is to get a large extent of the laminar boundary layer taking also into account the other design objectives and the different off-design conditions occuring on transport aircraft [20]. The extent of laminar flow on a swept wing is limited by three different mechanisms of transition into turbulent flow, described before. For each of these three instability modes certain types of favourable pressure distributions exist. In order to get a good compromise of pressure distribution between contrary demands from the viewpoint of the different stability modes it is of basic interest to investigate the influence of the pressure distribution on the different types of instability.

Fig. 4 shows the limit pressure distributions for different Reynolds numbers for Tollmien-Schlichting instability. Transition is prescribed to occur at the beginning of the steep pressure rise at nearly 60 % of chord length for the three pressure distributions. At low Reynolds numbers the laminar flow is able to overcome a certain pressure rise. At constant pressure the transition Reynolds number in free flight may have values of five to eight million indicated by a chord length Reynolds number of ten million in Fig. 4. At higher Reynolds numbers the flow has to be more and more accelerated to keep the boundary layer laminar.

Additionally the shape of the pressure distribution has a strong influence on transition behaviour. Fig. 5a shows a conventional convex pressure distribution in comparison with a more front-loaded one. The front-loaded pressure distribution type

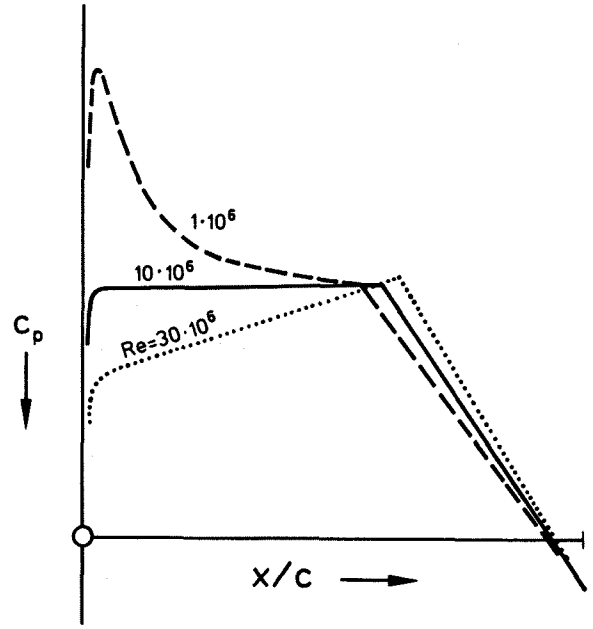

Fig. 4 Limit pressure distributions for laminar flow for different Reynolds numbers

induces remarkable higher amplification rates of TS-waves in the forward part of the laminar flow region but near the pressure minimum it results in a lower amplification ratio or N-factor than the conventional type as shown in Fig. 5b.

If the amplification ratio curve of the front-loaded type reaches the limiting line at which transition is assumed to occur the transition location moves rapidly upstream. For the conventional pressure distribution the transition location is moving slowly upstream with increasing angle of attack, but it already starts moving at lower angles of attack. This different transition behaviour leads to different types of laminar drag buckets shown in the drag polar curve in Fig. 5c. The front-loaded type of the pressure distribution has a larger range of lift coefficients with minimum drag, but this range is limited by a steep drag increase. In the case of the conventional pressure distribution the laminar drag bucket is more rounded.

On swept wings the choice of sweep angle is depending on the crossflow instability. The steep pressure drop at the leading edge produces large crossflow velocities with large amplification ratios as shown in Fig. 6a. In the following region of constant pressure no spanwise pressure gradients exist. Thus, the crossflow velocities disappear and thereby the instability, too. With increasing Reynolds number the amplification ratio grows until at least a certain limiting N-factor is reached and transition occurs.

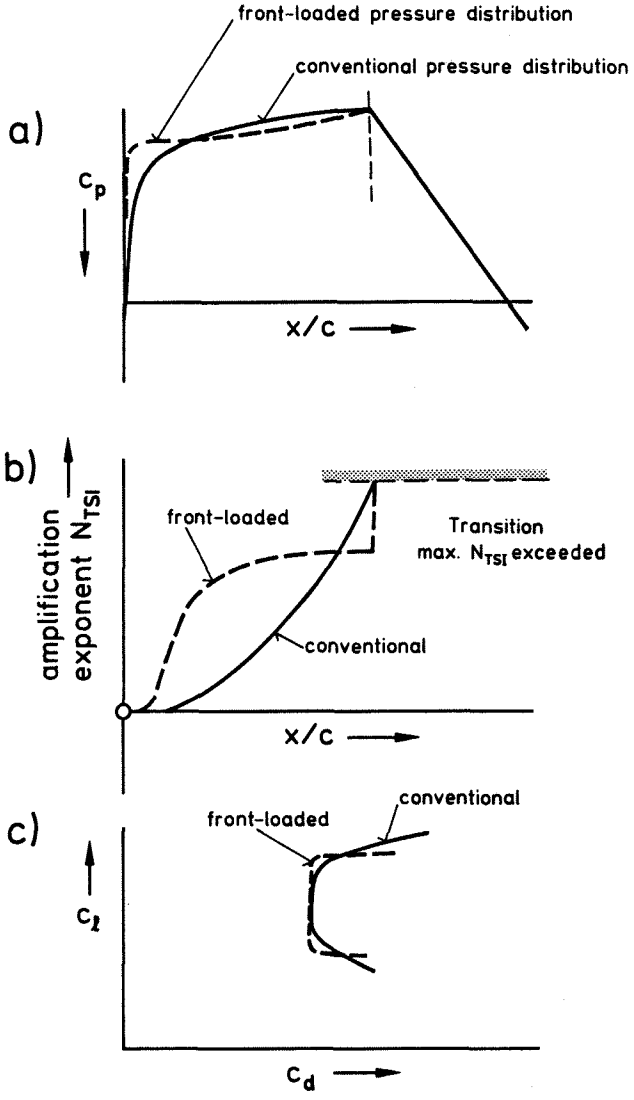

Fig. 5 Effect of pressure distribution on amplification exponent N_{TSI} and drag polar

The effect of sweep angle can be seen in Fig. 6b. With increasing sweep angle the pressure drop is reduced, but because of the increasing crossflow component the amplification ratio becomes larger.

The effect of slight flow acceleration downstream of the steep leading edge pressure drop is given in Fig. 7a. Near the leading edge the N-factor grows rapidly caused by the steep pressure drop. In the following region of slight acceleration the N-factor is decreasing and then more downstream slightly increases again caused by different wave lengths.

Fig. 7b shows the influence of leading edge pressure distribution on the growth of crossflow waves. The more rounded type, designated as conventional pressure dis-

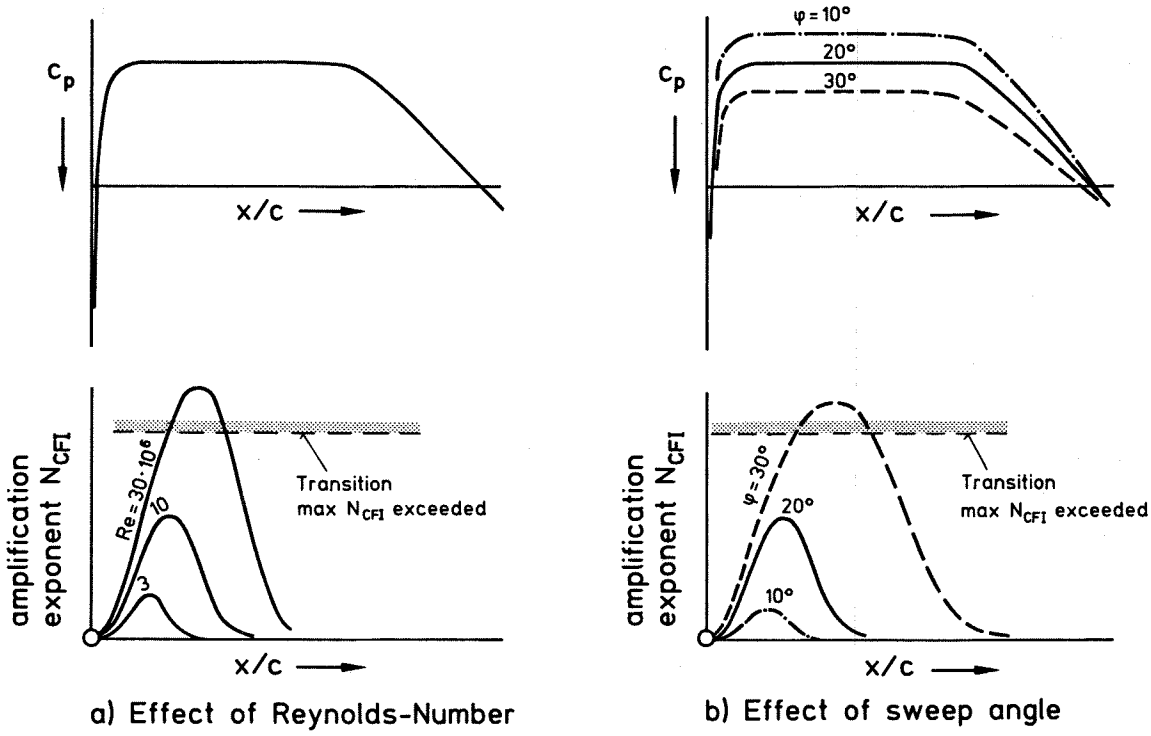

Fig. 6 Effect of Reynolds number and sweep angle on amplification exponent N_{CFI}

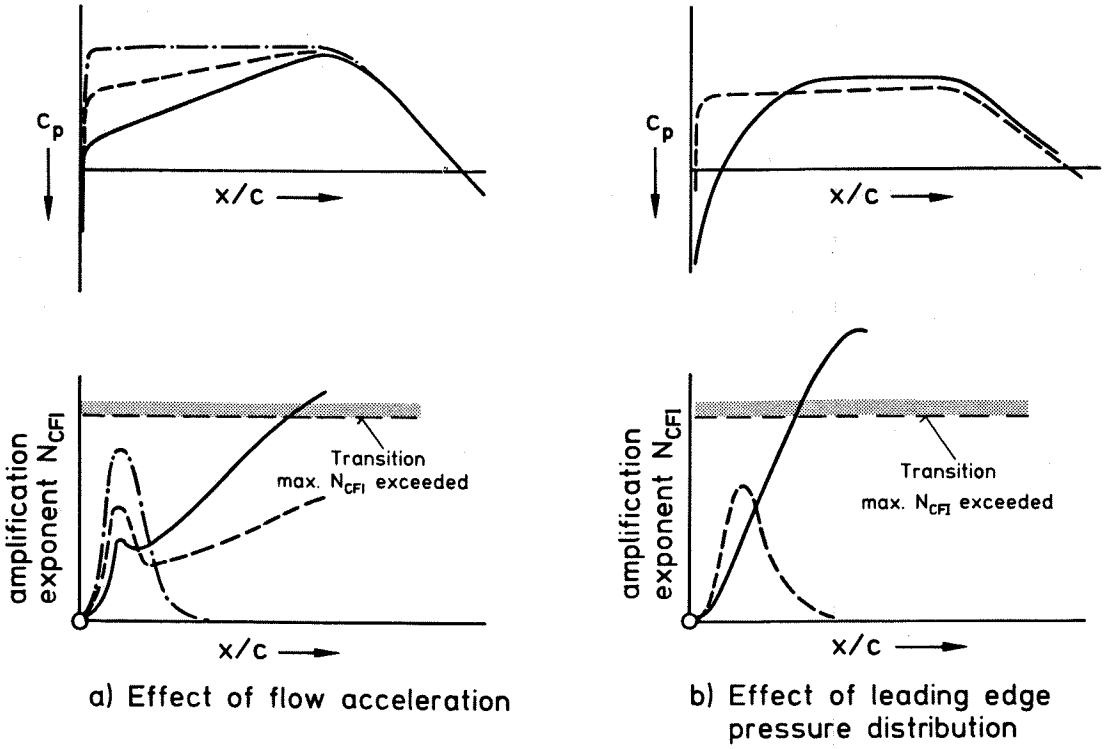

Fig. 7 Effect of flow acceleration and leading edge pressure distribution on amplification exponent N_{CFI}

tribution induces an increasing amplification ratio in the whole laminar flow region. The more front-loaded pressure distribution shows at first a stronger growth of the amplification ratio, but further downstream the crossflow becomes stable caused by the nearly constant pressure. It is remarkable that the maximum amplification ratio of the front-loaded pressure distribution is clearly lower than that of the conventional one.

On a wing the possibility of transition by Tollmien-Schlichting instability and by crossflow instability leads to a transition behaviour as shown in Fig. 8, where dependent on the lift coefficient the chordwise transition location is plotted for the upper and lower surface. Starting from the design lift coefficient in the middle of the laminar bucket of an unswept wing in Fig. 8a the upper limit of the laminar bucket is given by the upstream mowing transition location on the upper surface at increasing angles of attack. The lower limit is given by the transition location on the lower surface at decreasing angles of attack. Fig. 8b shows that in the case of a swept wing each surface has its own laminar bucket. On the upper side e.g. the upper limit is given in the same manner as described in Fig. 8a. The lower limit is given by crossflow induced transition which is caused by the more and more rounded leading edge pressure distribution with decreasing angles of attack. In a similar way a laminar bucket for the lower surface can be constructed. The upper limit is given by transition due to crossflow instability while the lower limit results from a transition by a Tollmien-Schlichting instability. Based on these considerations the presented drag polars can be explained. On a well designed airfoil the laminar buckets of both sides should have the same limits of lift coefficient.

At last the mechanism of attachment line transition has to be taken into account. Following the criterion mentioned in section 3.1, given in [6] and [7], the attachment line transition will be forced by:

- large sweep angles
- large Reynolds numbers
- small flow acceleration at the leading edge.

The same design features which prevent transition by crossflow instability seem

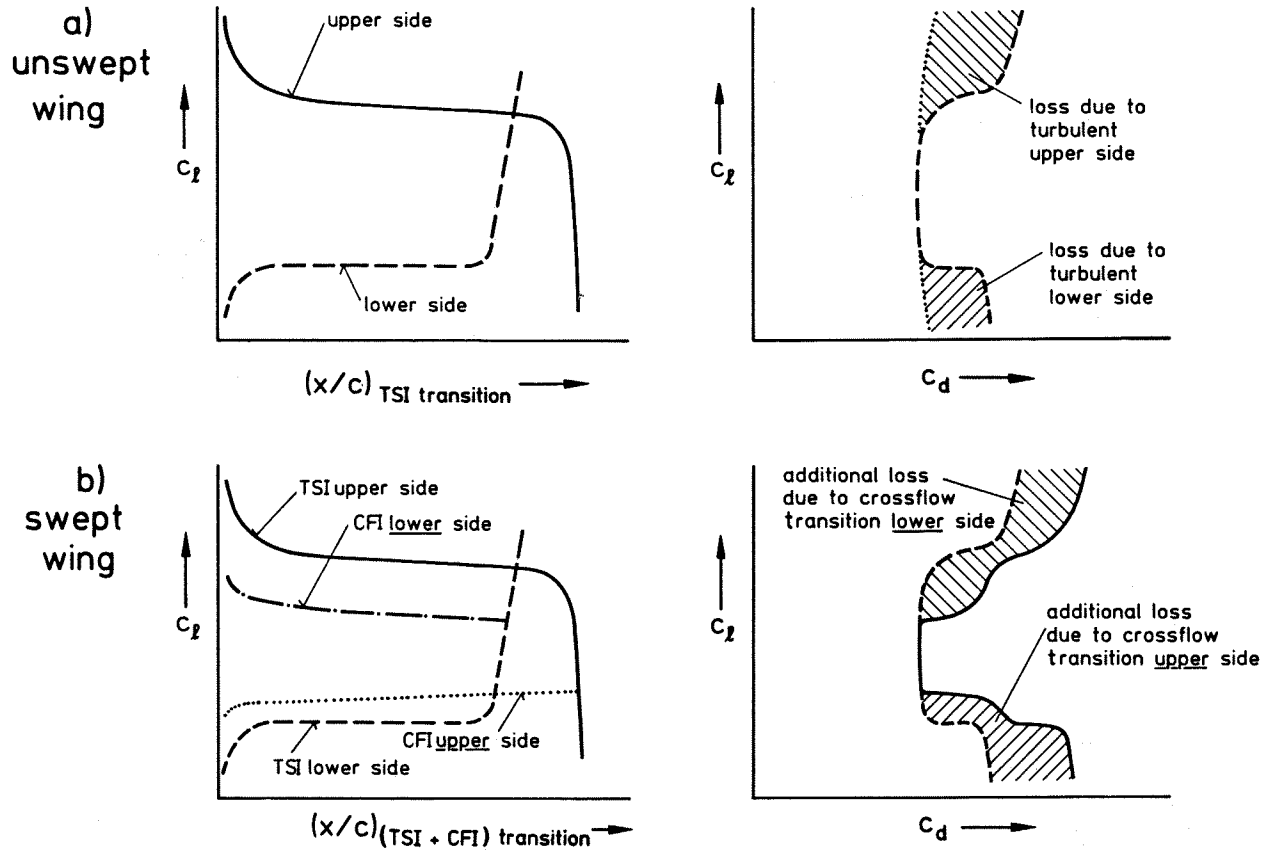

Fig. 8 Position of transition and schematic drag development as function of lift
a) unswept wing: transition due to TSI
b) swept wing: transition due to TSI and CFI

also to be favourable to prevent attachment line transition. The airfoil calculations presented in this paper indicate that the attachment line transition do not occur if the transition by crossflow is prevented.

Combining the design features of TSI, CFI and ALT the following arrangement of the pressure distribution seems to be necessary for a natural laminar flow airfoil for transport aircraft with swept wings:

- steep pressure distribution at the leading edge (favourable for CFI and ALT),
- followed by a small region of constant pressure or even a slight, small pressure rise (favourable for CFI) and
- followed by a concave pressure distribution with slight acceleration until the steep pressure rise with turbulent boundary layer (favourable for TSI).

3.3 Design objectives and airfoil design

The design objectives for a transport aircraft wing are given by the following values:

Flight Mach number	$M_F = 0.8$
Reynolds number	$Re = 30 \cdot 10^6$
Sweep angle	$\varphi = 22^\circ$
Lift coefficient	$c_L = 0.5$

This leads to the design values of a basic airfoil with:

$$M = 0.74$$
$$Re = 26.5 \cdot 10^6$$
$$c_\ell = 0.6$$

Taking into account these design objectives and the design features described in 3.2 a natural laminar airfoil DFVLR-LV2 was designed with a thickness of 11.7 % [21,22]. The pressure distribution is shown in Fig. 9. The laminar flow region is extended until 65 % of chord length on the upper surface and 60 % on the lower surface. The supersonic field on the upper surface is closed by a weak shock. The shock strength is so small that the calculations do not give an additional wave drag.

Fig. 10 shows calculated drag- and lift coefficient polar curves for the design Mach number M = 0.74 taking into account transition due to Tollmien-Schlichting instability as well as crossflow instability. The transition location in these calculations is given by the SALLY-code with an assumed maximum logarithmic amplification exponent of $N_{TSI} = 18$ for Tollmien-Schlichting waves and $N_{CFI} = 12$ for crossflow waves. At the upper limit of the laminar bucket the upper surface becomes turbulent by TSI and the lower surface by CFI, whereas

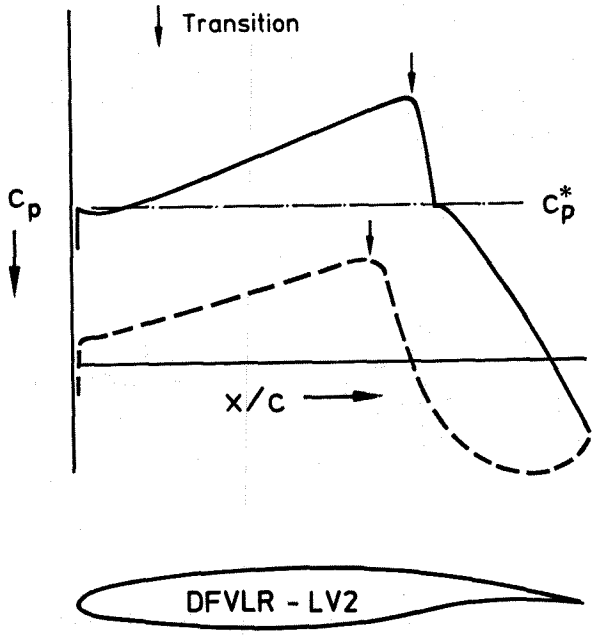

Fig. 9 Pressure distribution and shape of transonic laminar airfoil DFVLR-LV2

at the lower limit the lower surface becomes turbulent by TSI and the upper surface by CFI. The calculations give a minimum drag of $c_d = 0.0036$ and a width of the laminar bucket of $\Delta c_\ell \approx 0.2$. By means of a simple flap the bucket can be shifted to higher or lower lift coefficients. In comparison to this natural laminar flow behaviour the corresponding drag polar for the airfoil with fixed transition at 2 % chord length shows a remarkable increase in drag coefficient.

The lift coefficient versus angle of attack curve shows a strange behaviour in case of the natural laminar flow airfoil.

The lift curve slope inside the laminar bucket is steeper than outside the bucket. This behaviour is caused by the thinner boundary layer. The rapidly changing boundary layer thickness at the limits of the laminar bucket causes a very steep slope near the lower limit and an adverse slope near the upper limit. These typical discontinuities may cause problems in guidance and control of an aircraft.

4. Effect of natural laminar flow airfoils on aircraft performance

In order to judge the benefits of laminar airfoils one has to investigate the consequences on the aircraft performance. The performance of an aircraft can roughly be described by the ratio L/D times flight

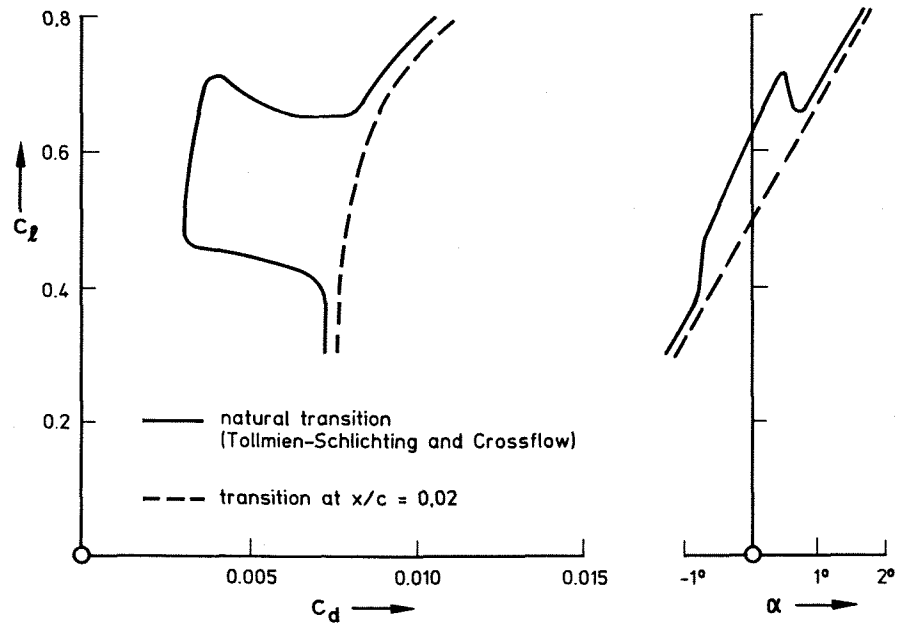

Fig. 10 Calculated lift and drag characteristics of laminar airfoil DFVLR-LV2 at $M = 0.74$, $Re = 26 \cdot 10^6$ and $\varphi = 22^\circ$

Mach number M_F. The ratio L/D represents the aerodynamic efficiency of the aircraft, i.e. the fuel consumption for a given flight distance, while the flight Mach number M_F takes into account the flight time. For comparison these values have been determined [21,22].

On the basis of the drag polars of a clean and contaminated laminar airfoil as shown for one Mach number in Fig. 10 the aircraft performance data have been calculated including the induced drag as well as the drag of the empennage and fuselage. The airfoils of the empennage have been assumed also to be laminar. The used drag coefficients of fuselage and empennage are given in Table 1.

In order to convert the airfoil data to wing data using simple sweep theory the airfoil lift coefficients are multiplied by the square of cosine of the sweep angle, whereas the drag coefficients remain unchanged. The flight Mach number is the airfoil Mach number divided by cos φ. The considered transport aircraft is of an AIRBUS-type and has a wing with a sweep angle of $\varphi = 22^\circ$ and an aspect ratio of $\Lambda = 8.8$.

Fig. 11 presents two c_L-M_F-diagrams with

drag	conventional aircraft	contaminated laminar aircraft	clean laminar aircraft
additional drag of slat	0.0005	0	0
empennage	0.0032	0.0032	0.0014
fuselage	0.0070	0.0070	0.0070
nacelle	0.0002	0.0002	0.0002
miscellaneous	0.0010	0.0010	0.0010
c_d parasite	0.0119	0.0114	0.0096

Tab. 1 Drag coefficients of fuselage, empennage, nacelle and miscellaneous

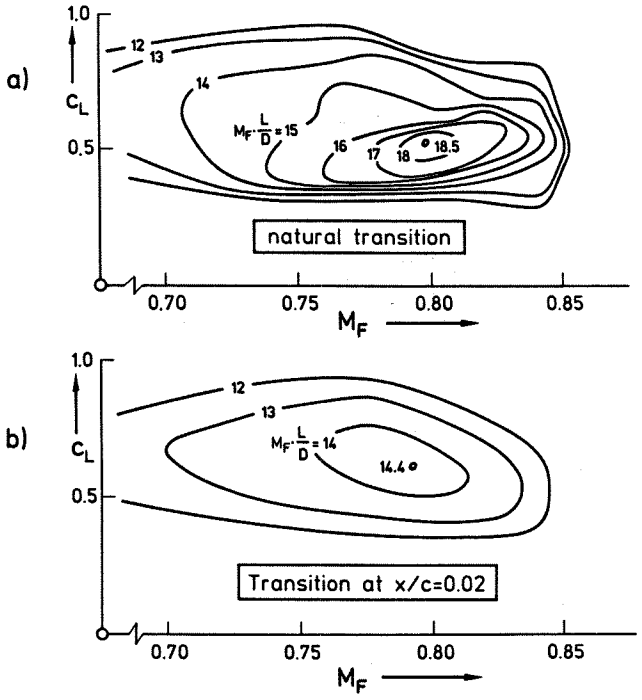

Fig. 11 Performance $M_F \cdot L/D$ of a transport aircraft with DFVLR-LV2 airfoil wing and sweep angle of $\varphi = 22^\circ$

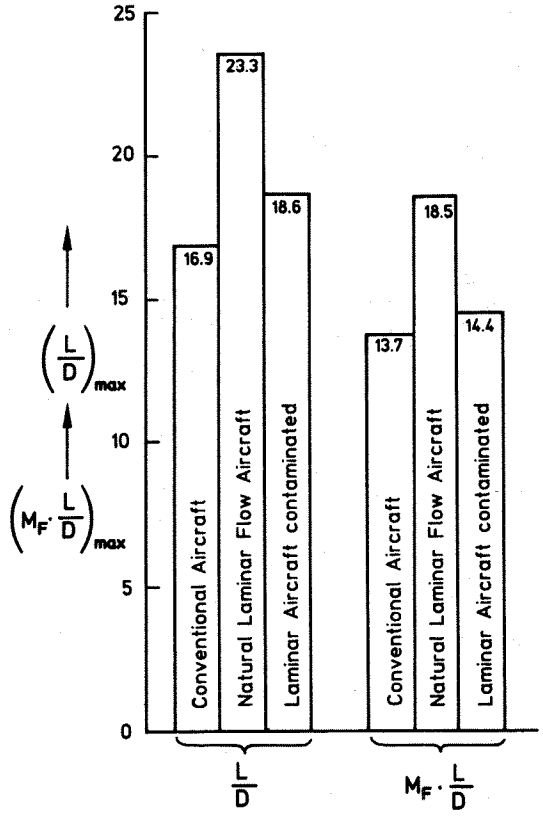

Fig. 12 Comparison of L/D and performance $M_F \cdot L/D$ of conventional aircraft and natural laminar flow aircraft

lines of constant performance $M_F \cdot L/D$ for comparing two essential cases: The "laminar aircraft" equipped with laminar wing and empennage (laminar boundary layer of 65 % chord on wing upper surface and 60 % on lower surface) but turbulent fuselage and an aircraft with contaminated wing and empennage (boundary layer transition assumed at 2 % chord for both surfaces). For the latter one there are smooth closed curves of constant $M_F \cdot L/D$ around a maximum value of $(M_F \cdot L/D)_{max} = 14.4$ at a Mach number of $M_F \approx 0.8$. Similar results (not shown) have been obtained for an aircraft with conventional wing and empennage. The wing is assumed to have the same weight as the laminar wing and therefore the wing sweep and the wing thickness are higher and the aspect ratio is lower. For the "laminar aircraft" the curves are not so smooth as a consequence of the drag polar of the laminar airfoil in Fig. 10 but show an essentially higher maximum of $(M_F \cdot L/D)_{max} = 18.5$ at a Mach number $M_F = 0.8$. This latter value demonstrates very clearly the remarkable improvement in performance for an aircraft with laminar wing and empennage.

A comparison of the maximum values of L/D and $M_F \cdot L/D$ for a conventional aircraft and the two cases of an aircraft with clean and contaminated laminar wing and empennage is given in Fig. 12. According to this the contaminated "laminar aircraft" is still a little more beneficial than the conventional aircraft. But one has to keep in mind that the cruise Mach number of the conventional aircraft is slightly higher. On the contrary the clean "laminar aircraft" shows about 30 % improved values of L/D (fuel consumption for a given distance) and $M_F \cdot L/D$ (performance) compared with the conventional one.

5. Problems associated with laminar flow on wings and experimental verification

Before realizing a laminar flow aircraft a set of problems has to be solved. The most critical and important one is the reliable prediction of transition location on wings in free flight at high Reynolds numbers.

In section 3 it has been pointed out that with the aid of the stability analysis of laminar boundary layers a transition location prediction seems to be possible by relating measured transition locations with calculated amplification ratios thus defining limiting values of N-factors for Tollmien-Schlichting instability as well as for crossflow instability. These limit values can only be derived from suitable and accurate experiments in free flight and wind tunnels.

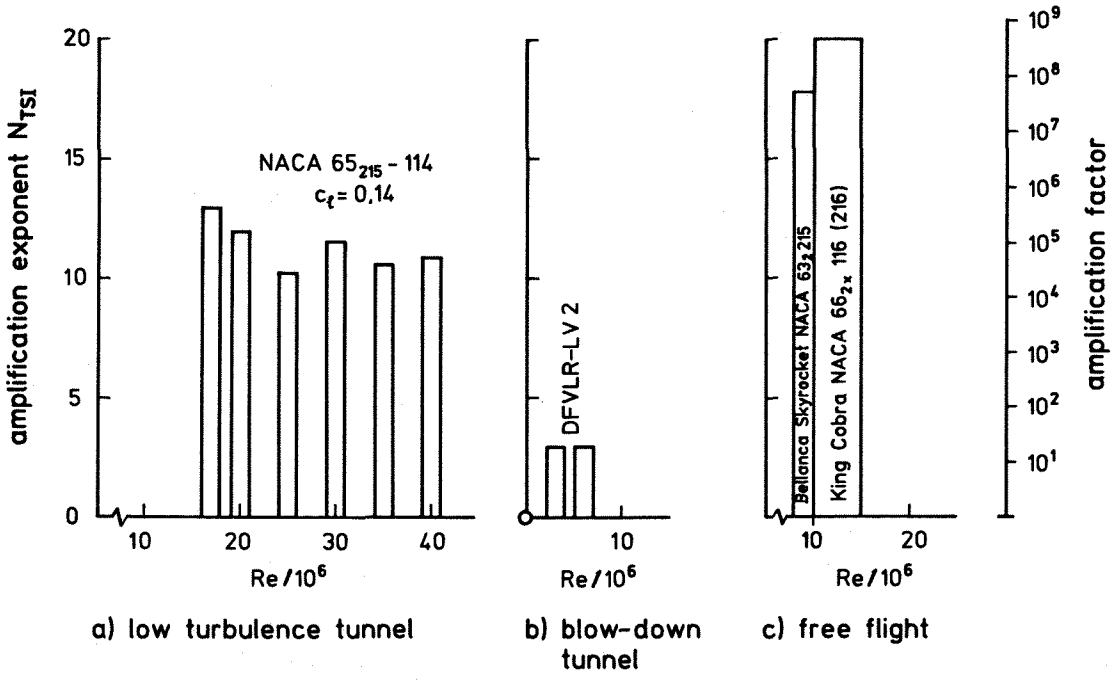

Fig. 13 Limit amplification exponents for Tollmien-Schlichting waves derived from free flight and windtunnel experiments

Fig. 13 shows the results of such analysis calculations with respect to Tollmien-Schlichting instability of published flight tests and windtunnel experiments in the Reynolds number range Re = $3 \cdot 10^6$ to $40 \cdot 10^6$ [23]. The amplification exponents N_{TSI} obtained from free flight tests at Reynolds numbers of 9 to $15 \cdot 10^6$ are of the order of $N_{TSI} = 20$, whereas the values of N_{TSI} from low turbulence windtunnel experiments at Reynolds numbers 17 to $40 \cdot 10^6$ lie between $N_{TSI} = 10$ and 13. Essentially lower values have been obtained from blow-down windtunnel tests at Reynolds numbers of 3 to $6 \cdot 10^6$. These values are only of the order of $N_{TSI} \approx 3$.

Micro-turbulence and noise in windtunnel flow being always present and dependent on the construction of the windtunnel and the achieved flow quality can be considered as possible reasons for the difference between the found amplification exponents from free flight and windtunnel tests. As a laminar boundary layer is strongly influenced by turbulence and noise premature boundary layer transition in windtunnels is observed. This can be confirmed by comparing the results of the limiting N_{TSI}-factors showing appreciably smaller N_{TSI}-values in blow-down windtunnels which proceduce higher levels of turbulence and noise than continuous low turbulence windtunnels. These windtunnel problems become evident in Fig. 14 which presents a comparison of one calculated and two measured drag polars for the laminar airfoil DFVLR-LV2. The calculations have been described in sect. 3.3. The experiments have been carried out in the Transonic Wind-

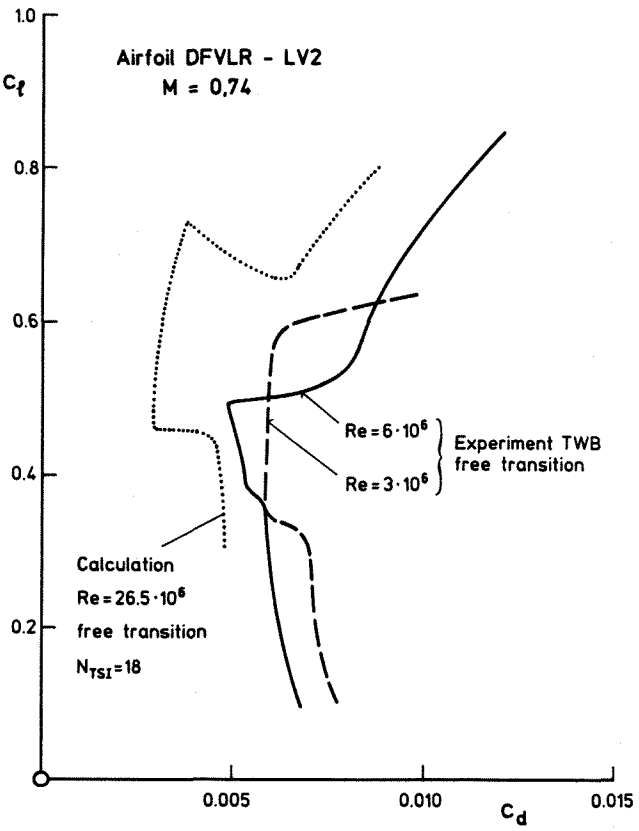

Fig. 14 Calculated and measured drag polars of airfoil DFVLR-LV2

tunnel Braunschweig (TWB) of DFVLR [24] with free transition at Reynolds numbers $Re = 3 \cdot 10^6$ and $6 \cdot 10^6$. For both Reynolds numbers the curves show a laminar bucket with considerable smaller drag coefficients compared with those which one would expect with fully turbulent boundary layer. But with increasing Reynolds numbers the bucket width decreases. At $Re = 9 \cdot 10^6$ the laminar bucket has disappeared (values not shown) but the calculation indicates, that even at $Re = 26.5 \cdot 10^6$ the laminar bucket with a width of $\Delta c_\ell \approx 0.2$ should exist. These experiments indicate quite clearly that it is possible to produce laminar boundary layers on airfoils at higher subsonic Mach numbers in this kind of windtunnel with pressure gradients which can be used for laminar airfoils at high Reynolds numbers. But is is also clear, that the amplification exponents N_{TSI} derived from these experiments (see Fig. 13) are too small as to allow long laminar boundary layers with corresponding low drag coefficients and wide laminar buckets at Reynolds numbers necessary for transport aircraft. The results in the Figures 13 and 14 underline that it is absolutely necessary to have

- transonic windtunnels with a high flow quality,
- reliable and accurate free flight tests and
- a correlation with respect to transition between windtunnel and free flight.

Besides the problems of airfoil development and experimental verification further difficulties exist, which should be briefly mentioned here.

- Replacement of slats by a more efficient trailing edge flap system.
- Problems with engine noise interaction with the laminar boundary layer.
- Smooth wing surface and small waviness.
- Contamination of the wing by insects and dust.

With respect to roughness (waviness, smoothness, contamination) theoretical considerations show that the permissible absolute height of surface roughness of transport aircraft wings has about the same order as sailplanes. Operational experiences with sailplanes for years indicate that despite of insect contamination the advantages of laminar airfoils have been proven.

6. Conclusions

Summarizing the results of the present paper the following statements can be made:

- The design of natural laminar flow airfoils for high Reynolds numbers and swept wings seems to be possible.
- Performance of transport aircraft with laminar wing and empennage is improved by 30 % compared to a conventional aircraft.
- The assumptions leading to these statements have to be validated with respect to transition prediction and experimental verification.
- Therefore suitable and reliable flight experiments have to be conducted at high Reynolds- and Mach numbers.
- On the other hand transonic windtunnels with high flow quality are indispensable.

References

[1] Schlichting, H.: Boundary-Layer Theory. 7. Edition, McGraw-Hill Book Company, New York (1979).

[2] Gray, W.E.: The effect of wing sweep on laminar flow. RAE TM Aero. 255, (1952).

[3] Owen, P.R.; Randall, D.J.: Boundary layer transition on the sweptback wing. RAE TM Aero. 277, (1952).

[4] Boltz, F.W.; Kenyon, G.C.; Allen, C.Q.: Effects of sweep angle on the boundary layer stability characteristics of an untapered wing at low speeds. NASA TN-D 338, (1960).

[5] Skrokowski, A.J.; Orzag, S.A.: Mass flow requirements for LFC wing design. AIAA Paper No. 77-1222, (1977).

[6] Pfenninger, W.: Laminar flow control. Laminarization. AGARD-R-654, (1977), pp. 3-1 to 3-75.

[7] Poll, D.I.A.: Transition in the infinite swept attachment line boundary layer. The Aeron. Quart. Vol. 30, (1979), pp. 607-629.

[8] Granville, P.S.: The calculation of the viscous drag of bodies of revolution. David Taylor Model Basin Report 849, (1953).

[9] Michel, R.: Critère de transition et amplification des ondes d'instabilité laminaire. La Recherche Aérosp. No. 70, (1979).

[10] Beasley, J.A.: Calculation of the laminar boundary layer and the prediction of transition on a sheared wing. ARC R&M 3787, (1973).

[11] Arnal, D.; Habiballah, M.; Coustouls, E.: Laminar instability theory and transition criteria in two- and three-dimensional flow. La Rech. Aérosp. No. 1984-2 (1984).

[12] Betchov, R.; Criminale, W.O.: Stability of parallel flows. Academic Press, New York, 1967.

[13] Mack, L.M.: Boundary layer stability theory. JPL Rep. No. 900-277 Rev. A. 1969.

[14] Dagenhardt, J.R.: Amplified Crossflow disturbances in the laminar boundary layer on swept wings with suction. NASA TP 1902 (1981).

[15] Gregory, N.; Stuart, J.T.; Walker, W.S.: On the stability of three-dimensional boundary layer with application to the flow due to a rotating disc. Phil. Trans. Roy. Soc. London, Series A, No. 943, Vo. 248, (1955), pp. 155-199.

[16] Runyan, J.; George-Falvy, D.: Amplification factors at transition on an unswept wing in free flight and on a swept wing in wind tunnel. AIAA-paper No. 79-0267, (1979).

[17] Jaffe, N.A.; Okamura, T.T.; Smith, A.M.O.: Determination of spatial amplification factors and their application to predicting transition. AIAA Journ., Vol. 8, (1970), pp. 301-308.

[18] Obara, C.J.; Holmes, B.J.: Flight-measured laminar boundary-layer transition phenomena including stability theory analysis. NASA TP 2417, (1985).

[19] Rohardt, C.H.: Erweiterung eines Nachrechnungsverfahrens für zweidimensionale Strömungen durch ein leistungsfähiges Grenzschichtverfahren. DFVLR-IB, (1983).

[20] – Hybrid laminar flow control study. Final technical report. (BOEING Commercial Airplane Co.) NASA CR 165930, (1982).

[21] Horstmann, K.H.; Köster, H.; Redeker, G.; Quast, A.: Laminarprofile für Verkehrsflugzeuge. DFVLR-IB, (1985).

[22] Horstmann, K.H.; Köster, H.; Redeker, G.; Quast, A.: Der Laminarflügel – Ein Weg zur Verbesserung der Wirtschaftlichkeit von Verkehrsflugzeugen. DFVLR-Nachrichten, Heft 46, (1985).

[23] Rohardt, C.H.: Anwendung eines Berechnungsverfahrens zur Ermittlung der Instabilitäten in der laminaren Grenzschicht im Hinblick auf die Bestimmung des laminar-turbulenten Umschlags an Profilen. DFVLR-IB, (1983).

[24] Stanewsky, E.; Puffert-Meißner, W.; Müller, R.; Hoheisel, H.: Der Transsonische Windkanal Braunschweig der DFVLR. Z. Flugwiss. Weltraumforsch. 6, (1982), pp. 398-408.